Geological Quarterly, 2022, 66: 11
DOI: http://dx.doi.org/10.7306/gq.1643

Further observations on the bio- and magnetostratigraphy of the J/K boundary interval in southern Ukraine

William A.P. WIMBLEDON[1], Andrea SVOBODOVA[2], Vladimir BAKHMUTOV[3], Ievgen POLIACHENKO[3] and Dmytro HLAVATSKYI[3]

[1] School of Earth Sciences, University of Bristol, Wills Memorial Building, Queens Road, Bristol BS8 1RJ, United Kingdom

[2] Czech Academy of Sciences, Institute of Geology, Rozvojová 269, 165 00 Prague, Czech Republic

[3] National Academy of Sciences of Ukraine, Institute of Geophysics, Palladina Av. 32, 03142 Kyiv, Ukraine

Wimbledon, W.A.P., Svobodova, A., Bakhmutov, V., Poliachenko I., Hlavatskyi, D., 2022. Further observations on the bio- and magnetostratigraphy of the J/K boundary interval in southern Ukraine. Geological Quarterly, 2022, 66: 11, doi: 10.7306/gq.1643

This is an account of finds of stratigraphically useful calcareous nannofossils and the magnetostratigraphy of the Jurassic-Cretaceous boundary interval of the eastern Crimean peninsula (southern Ukraine). We compare these new complementary results with those presented by our team in earlier publications. A missing interval in the Crimean sequence is filled, and the position of the Tithonian-Berriasian (J/K) boundary is confirmed.

Key words: J/K boundary, Tithonian, Berriasian calcareous nannofossils, magnetostratigraphy.

INTRODUCTION

In this contribution we give an account of a short stratigraphic interval just below the Jurassic/Cretaceous boundary in eastern Crimea. This interval has not previously been noticed and its description here fills a gap in knowledge of the Tithonian-Berriasian, and describes an interval not noticed in our earlier publications on the region (Bakhmutov et al., 2016; Wimbledon et al., 2017b, 2020a; Svobodová et al., 2019a).

In 2016 it was agreed, and announced at the International Cretaceous Symposium in Vienna, that the base of the Berriasian Stage (and the Cretaceous System) was to be placed at the base of the *Calpionella alpina* Subzone, adopting the marker and level most frequently applied by authors in the previous decade. After documentation and consideration of numerous sites in Europe, Africa, North and South America and Asia, the Berriasian Working Group (ISCS, International Commission on Stratigraphy) held a formal vote, and accepted by a 76% majority that the base of the Alpina Subzone should be selected as the primary marker for the Tithonian/Berriasian boundary. In the judgment of the 75-strong group of J/K specialists, the calpionellid turnover at this level provided the best marker, and, compared to other less-satisfactory putative markers, was the one that allowed correlation over the greatest part of the globe (Wimbledon et al., 2017a, 2020b).

However, after more than ten years of study of sections in central and eastern Crimea, our team concluded, with regret, that the refined calpionellid-based zonation that had been so successfully applied at numerous sites in Tethys, extending to North and South America, could not be made to work in southern Ukraine (see Bakhmutov et al., 2018 for details). Thus our focus in Crimea shifted to the application of calcareous nannofossils with magnetostratigraphy, and subsidiary ammonites.

Literature on J/K calcareous nannofossils in Crimea is limited. Following on from our own reconnaissance studies and those published by Matveev (2009) and Matlai (2011), Ivanik et al. (2013) made no mention of nannofossils in their radical interpretation of the Theodosia sequence (below and just west of the southern lighthouse) which they related only to Russian ammonite biostratigraphy. In preliminary works (Bakhmutov et al., 2016; Wimbledon et al., 2017b), a revised stratigraphy was given of the same beds in the cliffs and foreshore on the south side of the headland of Ili Burnu and further north to the town of Theodosia. The next paper (Bakhmutov et al., 2018) gave a fuller account of the upper Dvuyakornaya and the Mayak formations, their nannofossils and magnetozones, together with foraminifera and limited data on calpionellids. Next, a lower stratigraphic interval some 3 km further west was assessed (Svobodová et al., 2019a). A commentary on these studies then appeared (Arkadiev et al., 2019), and this was followed by a reply from our team – taking the opportunity to compare results from the Ukrainian succession with those won at numerous other Tethyan sites (Wimbledon et al., 2020a).

One other publication has appeared recently that mentions calcareous nannofossils (associated with planktonic fora-

* Corresponding author, e-mail: asvobodova@gli.cas.cz

Received: November 18, 2021; accepted: March 21, 2022; first published online: June 16, 2022

minifera) from southern Ukraine (Gradstein et al., 2019) – collected from a carbonate "interval across the Jurassic-Cretaceous boundary" at Krasnosilivka, south of Belogirsk. Some of the listed species were noted as characteristically lower Cretaceous (e.g., *Cruciellipsis cuvillierii* [*sic*]), and loosely assigned to the ammonite Jacobi Zone, though the Jacobi Zone has its base in the Tithonian: *Berriasella jacobi* is not present at that low level and is thus not a basal marker for the zone or the Berriasian (Frau et al., 2016). The bottom of the road section south of Krasnosilivka is marked by a major stratigraphic break: a conglomerate rests on an angular unconformity, with siliciclastics above, and then the first few metres of the carbonate succession (isolated from the rest). The lithostratigraphic level of the Gradstein et al. (2019) sample is not clear (the coordinates given are in the village, not on the roadside outcrops that extend up to 2 km further south): the cited nannofossils appear to indicate a horizon well above the base of the stage (and the section). The listing of "*Retecapsa angustiforata*" indicates a level, at the oldest, in mid M17r. *Cretarhabdus angustiforatus* (Black) has not so far been recorded in the presumed equivalent levels of the Mayak Formation on the Theodosia coast.

LOCALITIES

The upper Tithonian-lower Berriasian succession of Crimea is perhaps the thickest in Europe. However, this contribution describes only a small part of that succession, a cliff section (Fig 1: section 3) south of Theodosia, on the Black Sea shore just west of the Ili Burnu headland (45°00'37"N, 35°25'10"E). Herein we give details of this "missing" interval (Fig. 1: section 3) that we were unable to describe in our 2018 account (Bakhmutov et al., 2018), because slope deposits covered (and still cover) this part of the sequence. The described locality and related sites are shown on the map (Fig. 2).

The cliff lies between two prominent outcrops of a massive 2m+ breccia bed. The eastern of these exposure defines the base of the main Ili Burnu section and the other (~300 metres further west) forms reefs in the littoral zone. We believe the newly studied cliff sequence (Fig. 1: section 3) lies stratigraphically above the 2 m breccia and for the most part below units in the main exposures at Ili Burnu (that is, the Gulley section: outcrop 2, Fig. 2, Wimbledon et al., 2020a). At Ili Burnu, at the base of the ~100 m Tithonian-Berriasian section is at the base of the prominent 2 m thick breccia mentioned above (section 1, Bakhmutov et al., 2018; outcrop 1, Fig. 2; Wimbledon et al., 2020a). This unfossiliferous rudstone unit was previously used by Russian workers as a convenient base for the Cretaceous System.

To reiterate, the "new" section represents the unexposed interval between the Breccia section (Fig. 2, outcrop 1; Wimbledon et al., 2020a) and the Gulley section (outcrop 2; Bakhmutov et al., 2018, section 2), where we tentatively placed the Tithonian-Berriasian boundary. That placing was founded on the incomings of the taxa *Nannoconus steinmannii minor, N. kamptneri minor* and *N. wintereri,* in a normal magnetic interval taken to be M19n.2n.

The sections discussed in this work (and shown in Fig. 1) are all part of the upper Dvuyakornaya Formation, a unit comprising thick mudstones punctuated by numerous grainstones/microbreccias of all thicknesses, with a lesser number of coarser breccias, and a few micrite beds. We believe that the stratigraphic order of the four numbered sections shown in Figure 1 is as follows: 1, 2, 3 and 4.

The lowest interval considered in this account is in a cliff located three kilometres west of the Ili Burnu lighthouse (Fig. 1: section 1; 45°00'18.4"N, 35°23'09"E). Beds there, below a prominent thick breccia bed, with nannofossils and magnetostratigraphy, have already been described by us (Svobodová et al., 2019a). Unfortunately, the breccia that caps the section has no beds exposed in the slope above it. We have had persistent doubts that the two breccias (at Ili Burnu and here 3 km to the west) are, in fact, the same unit. The shore breccia bed can be traced westwards and identified with certainty for >1.5 km, but then outcrop fades. And the thicknesses of that very coarse breccia (Fig. 1: section 2) and the one in the western outcrop (Fig. 1: section 1) are not the same, and their clast sizes also differ. If they are not the same bed, then they are probably not very distant from one another stratigraphically, but the lack of exposure does not allow us to test this hypothesis. However, the evidence provided by nannofossil taxa gives age indications for the two, and this suggests that the western section is slightly lower in the Tithonian than the eastern outcrop (which is only just below the base of the Berriasian).

Arkadiev et al. (2019), in the 80 metres below the same breccia (their outcrop 2922), found no stratigraphically indicative nannofossil. Though the upper 25 metres had yielded to Svobodová et al. (2019a) a typical late Tithonian assemblage of *Nannoconus infans, N. puer* and *N. globulus minor, Polycostella* sp. and a single level containing a possible *Rhagodiscus asper*. The 25 m that yielded this assemblage straddles a reversed magnetic interval, below, and a normal interval: which we interpret as M19r and lowest part of M19n.2n.

About 140 metres below the breccia bed, Arkadiev et al. (2019) recorded isolated nannofossil finds that they interpreted as the FOs of *Nannoconus compressus* and *Polycostella senaria*. These species are noted in the literature as having their first occurrences well below both M19r and M19n, in the early Tithonian: respectively, in magnetozone M21n (*fide* Varol and Bowman, 2019) and magnetozone M20r (*fide* Bralower et al., 1989).

Figure 1 shows all the sections mentioned above, with ranges of selected nannofossils and magnetic polarity: the basal Breccia section (section 2), the Gulley section (section 4), described in 2018, the new profile (section 3) and the Tithonian section 3 km to the west (section 1).

CALCAREOUS NANNOFOSSIL INVESTIGATIONS

MATERIAL AND METHODS

Calcareous nannofossils were analysed in smear slides prepared by the decantation method using a 7% solution of hydrogen peroxide (methodology described e.g., in Švábenická, 2012) and mounted in Entellan. A total of 38 samples (22 FR samples and 16 MW samples) have been examined under and *Olympus BX53* light microscope using an immersion objective with a 100× magnification. Digital images of nannofossil specimens were made using an *Olympus UC90* digital camera.

In order to obtain the relative nannofossil abundances and semi-quantitative information about the respective calcareous nannofossil assemblages, 500 specimens were counted on each slide. Some samples did not provide so many specimens, so in those the number of all nannofossils found in 300 fields of view was used as the basis for interpretation (namely samples FR 13 and FR 15).

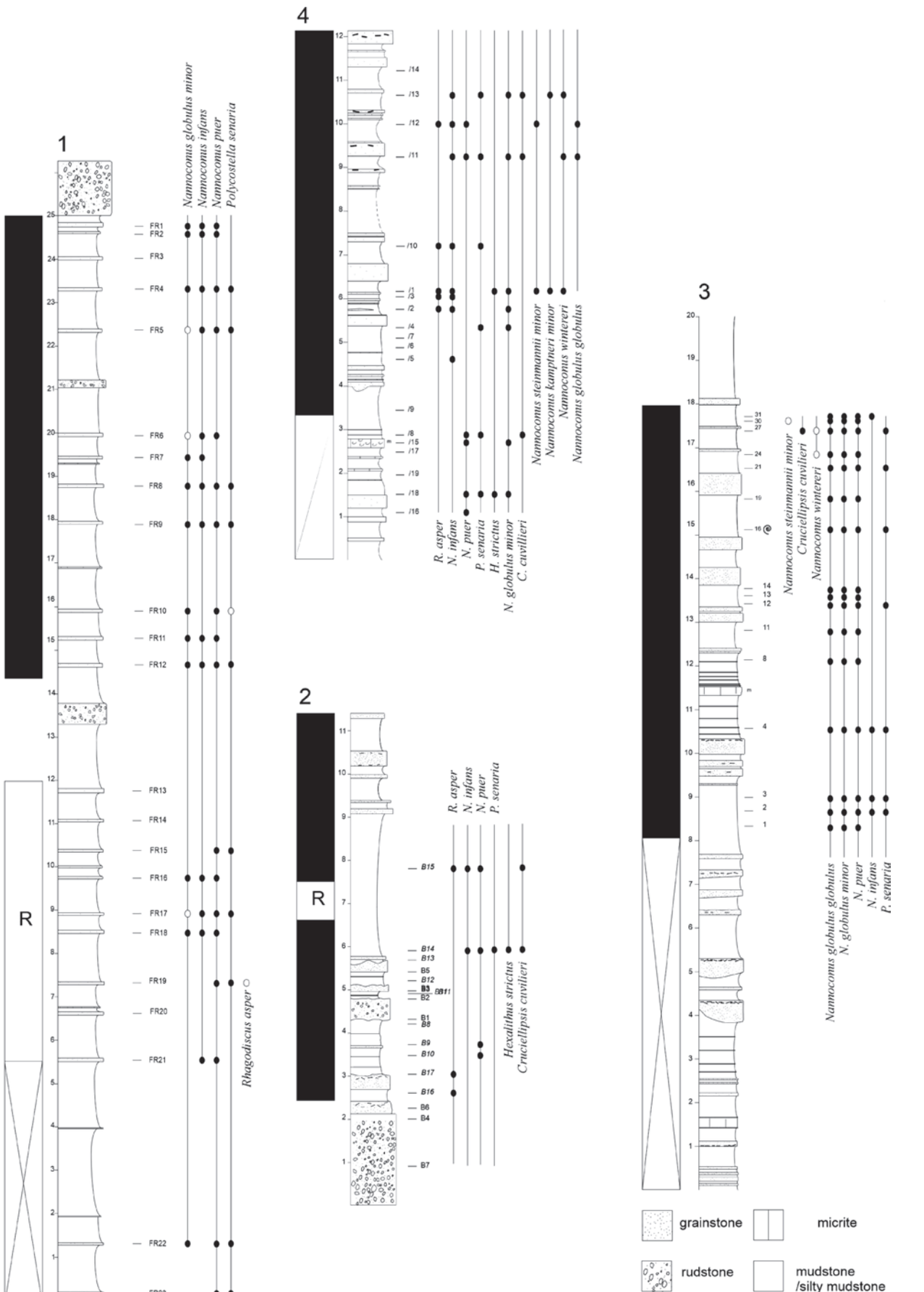

Fig. 1. Tithonian-Berriasian sections west from Ili Burnu

Ranges of selected nannofossil taxa and magnetic polarity are shown; **1** – after Svobodová et al. (2019) (45°00'18.4"N, 35°23'09"E); **2, 4** – Breccia and Gulley sections after Bakhmutov et al. (2018); **3** – shore cliff described herein (45°00'37"N, 35°25'10"E); "MW" sample points shown; ranges of selected nannofossil taxa and magnetic polarity (black – normal, white – reversed) are shown

Fig. 2. Locality map

1–4 – described sections

The identifications of species follow Bralower et al. (1989), Bown and Cooper (1998), Casellato (2010), Nannotax website (Young et al., 2017), Varol and Bowman (2019) and Casellato and Erba (2021). The smear slides are stored at the Institute of Geology of the Czech Academy of Sciences, Department of Paleobiology and Paleoecology.

RESULTS

In the samples studied, 60 calcareous nannofossils taxa have been identified. Their preservation ranges from moderate to very poor, heavily etched by dissolution. Also the abundance varies between high (up to 50 specimens per field of view), moderate (20–40 specimens per field of view), low (1–10 specimens per field of view) and very low (<1 specimen per field of view). All quantitative data, including information about preservation of calcareous nannofossils and individual abundances for each species per sample are given in Figure 3.

FR SAMPLES (FIG. 1: SECTION 1)

The most abundant components of the assemblage are the form genera *Watznaueria* (75% on average), *Cyclagelosphaera* (11% of the assemblage) and *Nannoconus* (nearly 7%). The genera *Conusphaera*, *Polycostella, Zeugrhabdotus* and other nannoliths and placoliths were found in small numbers.

As in the previous study from this area (Bakhmutov et al., 2018), older, redeposited, Jurassic nannofossils occur irregularly through the studied section (namely, the genera *Parhabdolithus*, *Lotharingius* and *Hexapodorhabdus*).

MW SAMPLES (FIG. 1: SECTION 3)

Similarly, as with section 1, the calcareous nannofossils are characterized by the dominance of *Watznaueria* (62% of the assemblage), *Nannoconus* (nearly 16%) and *Cyclagelosphaera* (>12% on average). *Conusphaera* reaches up to 5% of the assemblage total, and *Polycostella* is almost absent. The higher content of nannoconids (in several samples ~20% of the assemblage) suggests that this part of the studied section is located stratigraphically closer to the J/K boundary. This is supported by the continuous presence of *Nannoconus globulus globulus* through the whole section (in FR samples it is absent), by the appearance of *Cruciellipsis cuvillieri*, and also by the uncertain occurrence of *Nannoconus wintereri* and *N. steinmannii minor* in the upper part of the section. Percentage content of selected nannofossil genera is shown in Figure 4.

Section 1

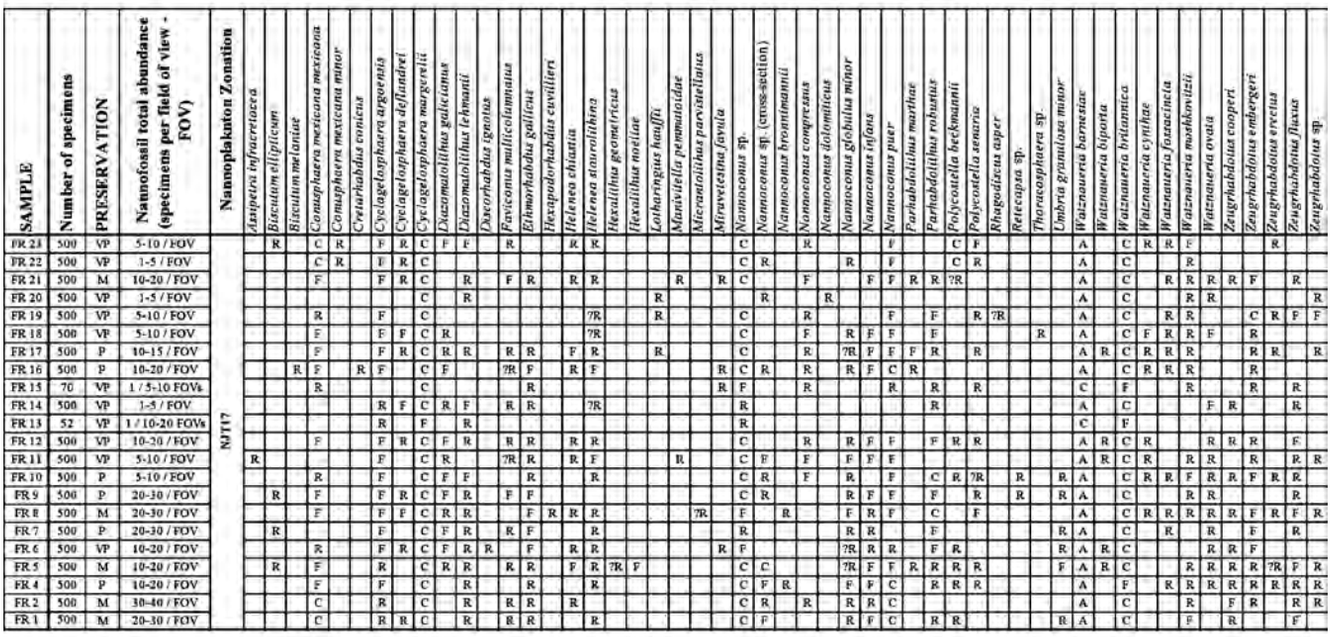

Section 3

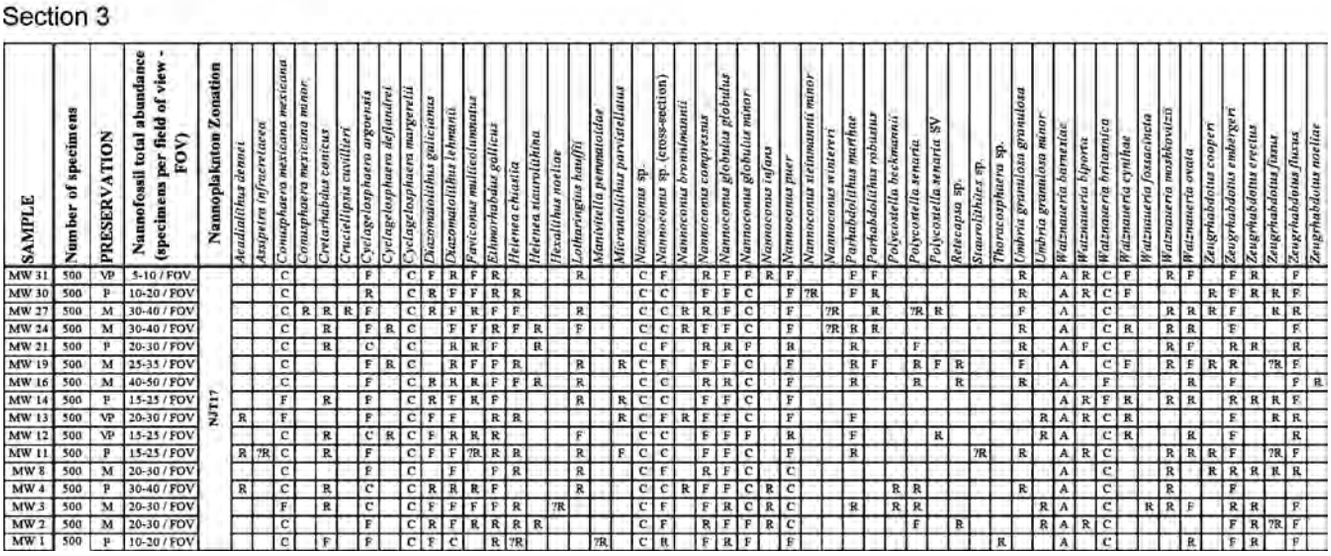

Fig. 3. Distribution of calcareous nannofosils in sections 1 and 3

Preservation of calcareous nannofossils is characterized using the abbreviations described by Bown (1992): VP (very poor) – extreme etching, P (poor) – strong dissolution, M (moderate) – moderate etching; the abundances for each species per sample were counted according to the classification proposed by Bown (1992): R (rare) – 1–2 specimens per sample; F (few) – 3–10 specimens per sample; C (common) – 11–100 specimens per sample; A (abundant) – >100 specimens per sample; calcareous nannofossil zonation follows Casellato and Erba (2021)

As in the FR samples (Fig. 1: section 1), older, redeposited, Jurassic taxa have been observed.

Selected calcareous nannofossil taxa are presented in Figures 5 and 6.

The list of calcareous nannofossil taxa present is given in Appendix 1.

THEODOSIA'S CALCAREOUS NANNOFOSSIL RECORD WITHIN THE GLOBAL STRATIGRAPHIC PATTERN

To appreciate how the Theodosia nannofossil records fit into wider palaeogeographic and stratigraphic pattern, it is necessary to consider other localities in other regions. Many nannofossil have enormously long stratigraphic ranges. Globally, some nannofossil species have their earliest occurrences (FOs) in the Tithonian, but there are also published records of FOs extending up into M19, through M19n, and crossing the base of the Cretaceous: this includes *Nannoconus puer* and *N. infans* (Wimbledon et al., 2020b: fig. 2; Figs. 7 and 8 herein – where source references are cited). In most modern accounts the lowest record of the FO of *N. globulus minor* is in M20n.2n and the lowest FOs of *Rhagodiscus asper* and *Cretarhabdus surirellus* in M19r. FO records of *Hexalithus strictus* are clustered in lower to middle M19n.2n. Clusters of the FOs of *Nannoconus wintereri* and *Cruciellipsis cuvillieri* in lower

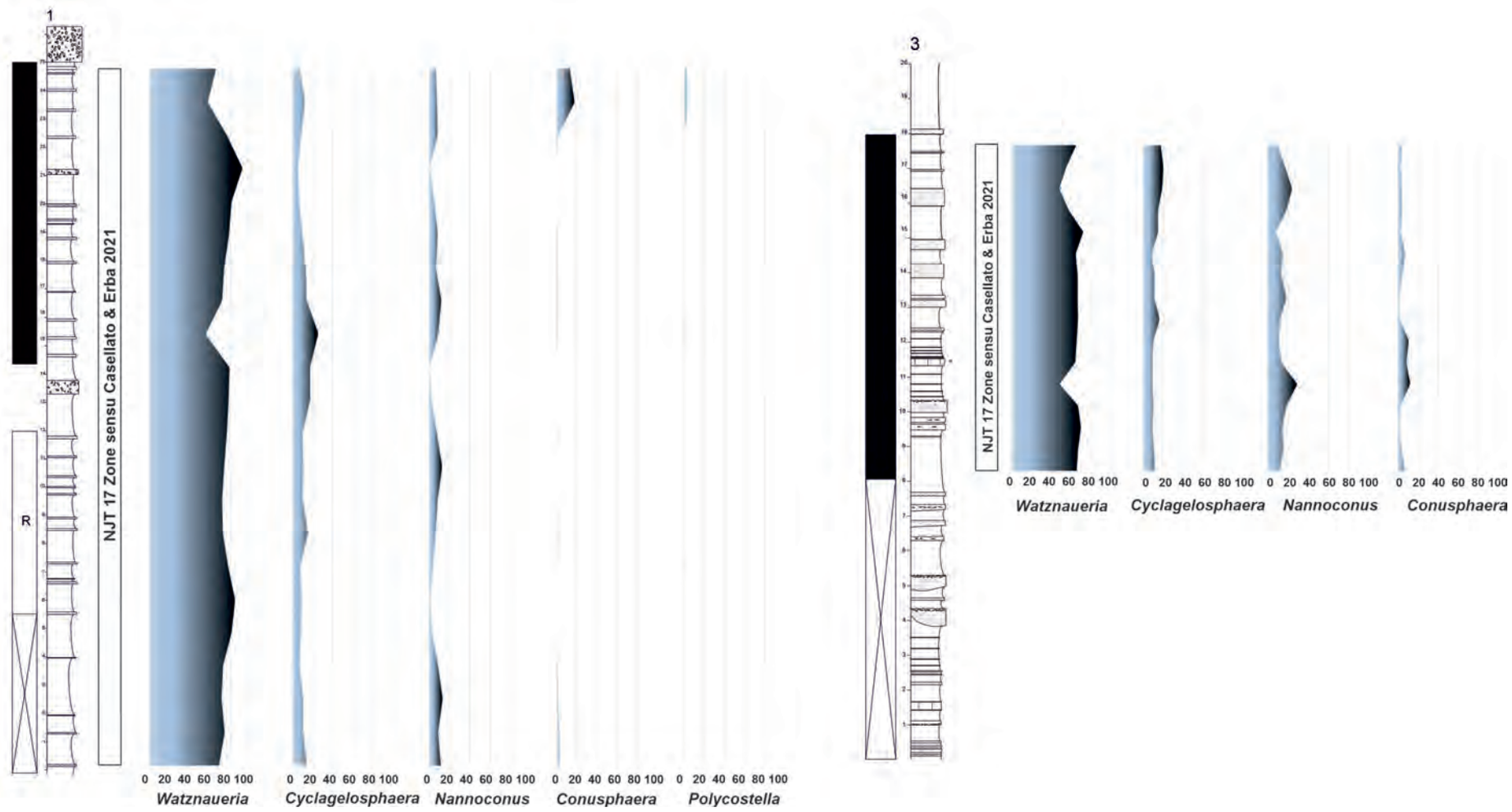

Fig. 4. Representation of selected nannofossil genera in sections 1 and 3 in percentage

Calcareous nannofossils zonation follows Casellato and Erba (2021)

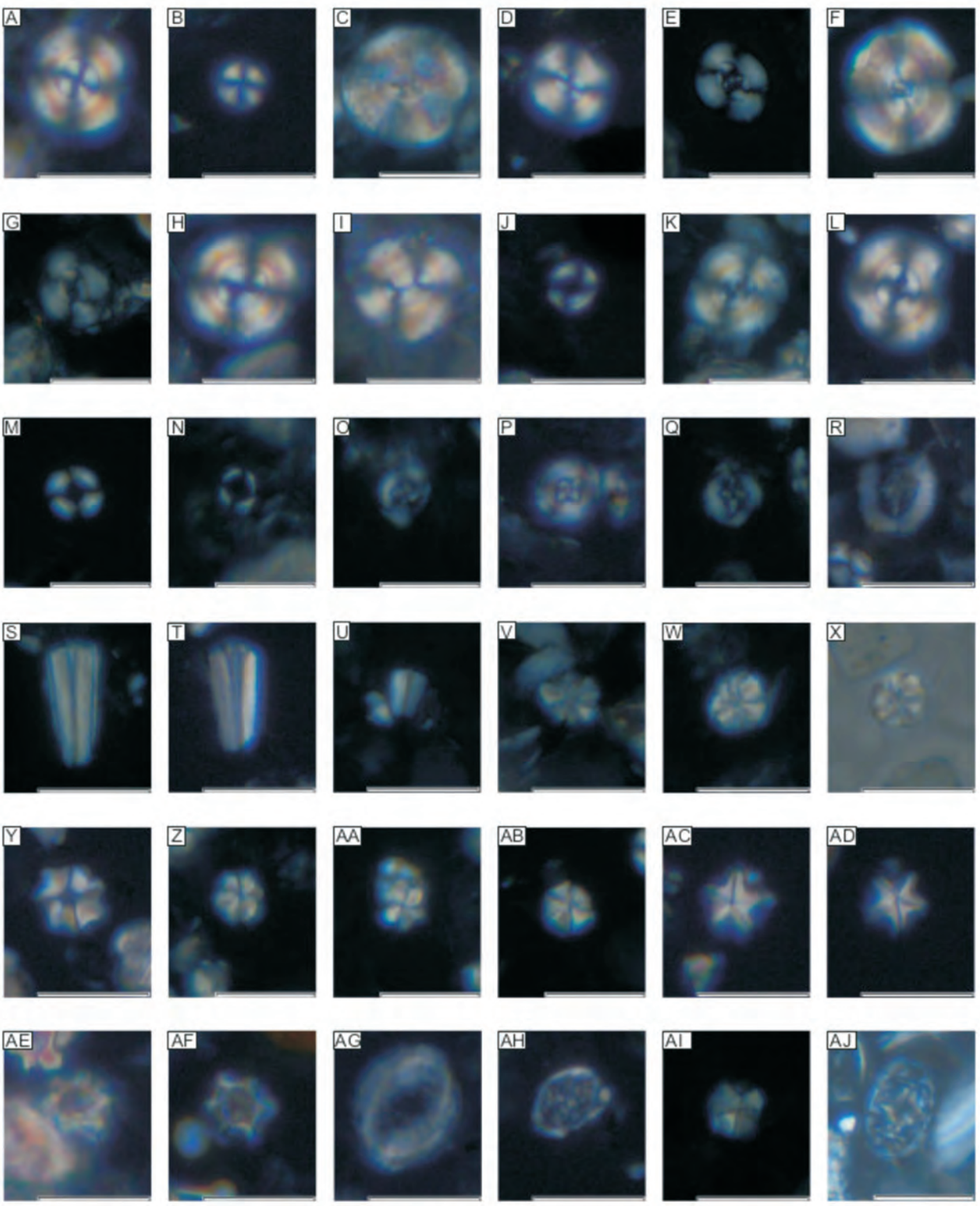

Fig. 5. Selected taxa of calcareous nannofossils from sections 1 and 3

A – *Cyclagelosphaera argoensis* Bown, 1992; sample MW 3, XPL; **B** – *Cyclagelosphaera margerelii* Noël, 1965; sample MW 2, XPL; **C** – *Cyclagelosphaera deflandrei* (Manivit, 1966) Roth, 1973; sample FR 9, XPL; **D** – *Watznaueria barnesiae* (Black in Black and Barnes, 1959) Perch-Nielsen, 1968; sample MW 3, XPL; **E, F** – *Watznaueria britannica* (Stradner, 1963) Reinhardt, 1964; samples FR 1, FR 10 (large specimen), XPL; **G** – *Watznaueria fossacincta* (Black, 1971) Bown in Bown and Cooper, 1989; sample FR 4, XPL; **H** – *Watznaueria biporta* Bukry, 1969; sample MW 13, XPL; **I** – *Watznaueria moshkovitzii* Varol and Bowman, 2019; sample MW 8, XPL; **J** – *Watznaueria ovata* Bukry, 1969; sample MW 3, XPL; **K, L** – *Watznaueria cynthae* Worsley, 1971; samples FR 8, MW 19, XPL; **M** – *Diazomatolithus lehmanii* Noël, 1965; sample FR 5, XPL; **N** – *Diazomatolithus galicianus* de Kaenel and Bergen, 1996; sample FR 7, XPL; **O**, **P** – *Helenea chiastia* Worsley, 1971; samples FR 5, MW 24, XPL; **Q** – *Helenea staurolithina* Worsley, 1971; sample FR 16, XPL; **R** – *Cretarhabdus conicus* Bramlette and Martini, 1964; sample MW 21, XPL; **S, T** – *Conusphaera mexicana* subsp. *mexicana* Trejo, 1969; samples FR 23, MW 19, XPL; **U** – *Conusphaera mexicana* subsp. *minor* Bown and Cooper, 1989; sample FR 23, MW 19, XPL; **V** – *Polycostella beckmannii* Thierstein, 1971; sample FR 12, XPL; **W, X** – *Polycostella beckmannii* Thierstein, 1971; sample FR 23, XPL, PPL (the same specimen); **Y** – *Polycostella senaria* Thierstein, 1971; sample MW 21, XPL; **Z, AA** – *Hexalithus noeliae* Loeblich and Tappan, 1966; sample FR 5, XPL; **AB** – ? *Hexalithus geometricus* Casellato, 2010; sample FR 5, XPL; **AC, AD** – *Polycostella parvistellatus* (Varol, 1991) Varol and Bowman 2019; samples MW 11, MW 19, XPL; **AE, AF** – *Acadialithus dennei* Howe, 2017; samples MW 4, MW 11, XPL; **AG** – *Ethmorhabdus gallicus* Noël, 1965; sample MW 19, XPL; **AH** – *Umbria granulosa* subsp. *granulosa* Bralower and Thierstein in Bralower et al., 1989; sample MW 19, XPL; **AI** – *Assipetra infracretacea* (Thierstein, 1973) Roth, 1973; sample FR 11, XPL; **AJ** – *Hexapodorhabdus cuvillieri* Noël, 1965; sample FR 8, XPL, XPL – cross polarized light, PPL – plane polarized light; scale bar represents 10 μm

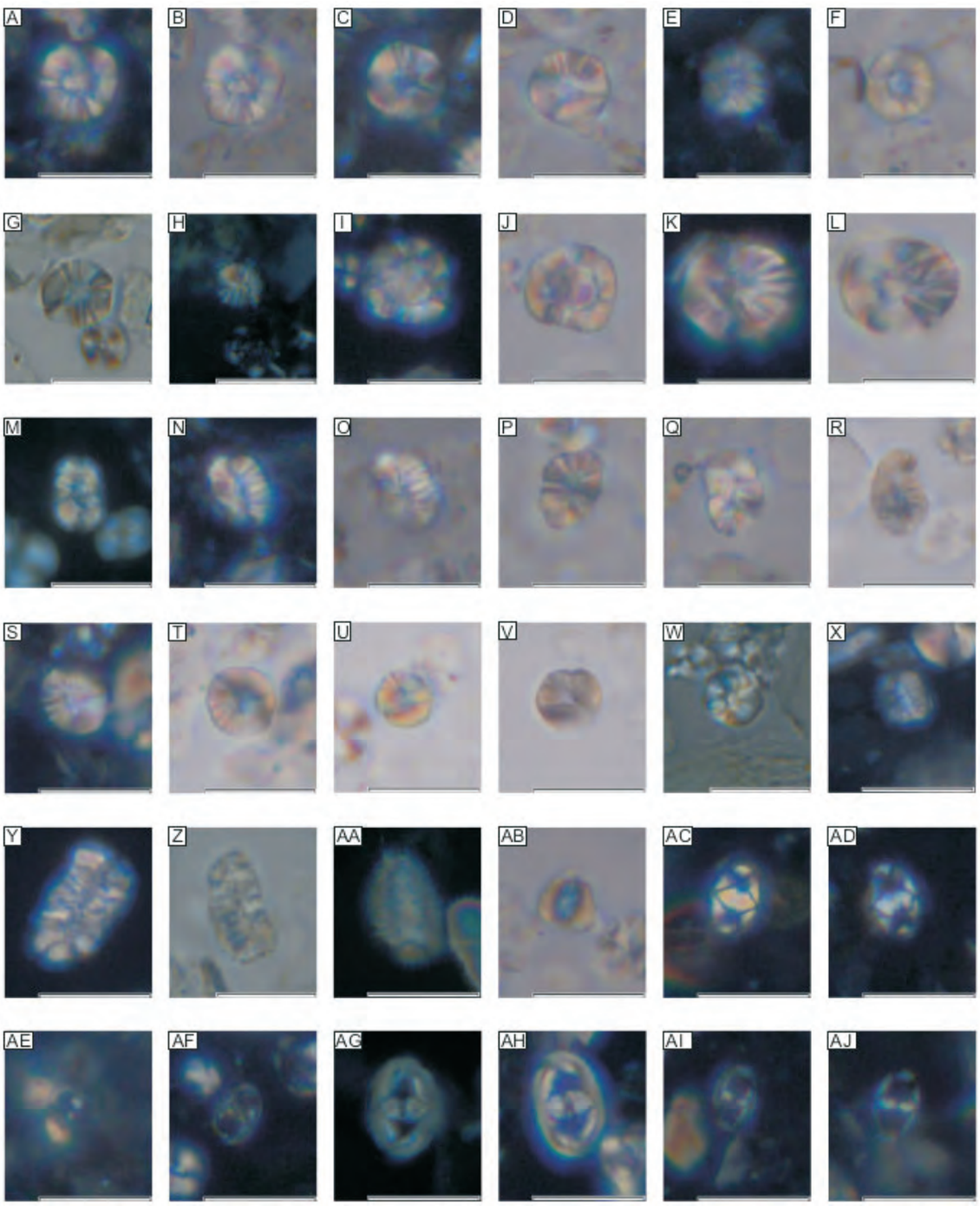

Fig. 6. Selected taxa of calcareous nannofossils from sections 1 and 3

A – *Nannoconus globulus* subsp. *minor* Bralower in Bralower et al., 1989; sample MW 1, XPL; **B** – *Nannoconus globulus* subsp. *minor* Bralower in Bralower et al., 1989; sample MW 1, PPL (the same specimen); **C** – *Nannoconus globulus* subsp. *minor* Bralower in Bralower et al., 1989; sample MW 8, XPL; **D** – *Nannoconus globulus* subsp. *minor* Bralower in Bralower et al., 1989; sample MW 8, PPL (the same specimen); **E** – *Nannoconus globulus* subsp. *minor* Bralower in Bralower et al., 1989; sample MW 14, XPL; **F** – *Nannoconus globulus* subsp. *minor* Bralower in Bralower et al., 1989; sample MW 14; PPL (the same specimen); **G** – *Nannoconus globulus* subsp. *minor* Bralower in Bralower et al., 1989; sample FR 1, PPL; **H** – *Nannoconus infans* Bralower in Bralower et al., 1989; sample FR 1, XPL; **I** – *Nannoconus globulus* subsp. *globulus* Brönnimann, 1955; sample MW 1, XPL; **J** – *Nannoconus globulus* subsp. *globulus* Brönnimann, 1955; sample MW 1, PPL (the same specimen); **K** – *Nannoconus globulus* subsp. *globulus* Brönnimann, 1955; sample MW 12, XPL; **L** – *Nannoconus globulus* subsp. *globulus* Brönnimann, 1955; sample MW 12, PPL (the same specimen); **M** – *Nannoconus compressus* Bralower and Thierstein in Bralower et al., 1989; sample FR 10, XPL; **N** – *Nannoconus compressus* Bralower and Thierstein in Bralower et al., 1989; sample MW 11, XPL; **O** – *Nannoconus compressus* Bralower and Thierstein in Bralower et al., 1989; sample MW 11, PPL (the same specimen); **P** – *Nannoconus compressus* Bralower and Thierstein in Bralower et al., 1989; sample MW 3, PPL; **Q** – *Nannoconus compressus* Bralower and Thierstein in Bralower et al., 1989; sample MW 12, PPL; **R** – *Nannoconus compressus* Bralower and Thierstein in Bralower et al., 1989; sample MW 19, PPL; **S** – *Nannoconus puer*, Casellato, 2010; sample MW 2, XPL; **T** – *Nannoconus puer*, Casellato, 2010; sample MW 2, PPL (the same specimen); **U** – *Nannoconus puer*, Casellato, 2010; sample MW 11, PPL; **V** – *Nannoconus puer*, Casellato, 2010; sample MW 19, PPL; **W** – *Nannoconus puer*, Casellato 2010; sample FR 2, PPL; **X** – *Polycostella senaria* SV (= *Nannoconus erbae* Casellato, 2010) Varol and Bowman, 2019; sample MW 27, XPL; **Y** – *Faviconus multicolumnatus* Bralower in Bralower et al., 1989; sample MW 19, XPL; **Z** – *Faviconus multicolumnatus* Bralower in Bralower et al., 1989; sample FR 5, PPL; **AA** – *Nannoconus dolomiticus* Cita and Pasquare, 1959; sample FR 20, XPL; **AB** – ? *Nannoconus wintereri* Bralower and Thierstein, in Bralower et al., 1989; sample MW 27, PPL; **AC, AD** – *Zeugrhabdotus cooperi* Bown, 1992; samples MW 11, MW 30, XPL; **AE** – *Zeugrhabdotus erectus* (Deflandre in Deflandre and Fert, 1954) Reinhardt, 1965; sample MW 30, XPL; **AF** – *Zeugrhabdotus noeliae* Rood et al., 1971; sample MW 16, XPL; **AG**, **AH** – *Zeugrhabdotus embergeri* (Noël, 1965) Perch-Nielsen, 1984; samples FR 19, MW 11, XPL; **AI, AJ** – *Zeugrhabdotus fluxus* Casellato, 2010; samples MW 11, MW 31, XPL, XPL – cross polarized light, PPL – plane polarized light; scale bar represents 10 μm

M20n.2n herald the approach of the base of the Alpina Subzone and the J/K boundary, with *Nannoconus steinmannii minor* providing the best proxy for the Alpina Subzone base and the base of the Berriasian, with a cluster here of its FOs. *Nannoconus kamptneri minor* FO records for the most part cluster in upper M19n.2n, continuing into M19n.1n, providing an upper limit for the immediate boundary interval. At Theodosia, occurrences of species FOs are indicated with a yellow circle in Figure 7. The stratigraphic positions compare well with those in more modern accounts of sites in other regions.

Here we consider stratigraphically indicative nannofossil FOs and not nannofossil biozones, as these are in a state of flux and have not yet stabilised: zones have sometimes been applied in publications without taking into account published changes in the positions of marker species, e.g. in Crimea, Arkadiev et al. (2019), citing and applying Bralower (1989) and Casellato (2010). Figure 8 shows how several taxa used as zonal indices now have very different positions and ages compared to those that were firstly, and subsequently, attributed to them.

Here we put the emphasis on first occurrences of nannofossil species. A number of nannofossil species are efficacious as indicators of stratigraphic level (Figs. 7 and 8): where such markers can be calibrated with calpionellid and magnetic datums, and ammonites, these can be consistent and most useful. But less trust can be placed in older results with lower resolution and on data from sections with poor or aberrant calpionellid records (e.g., Torre de' Busi, Figs. 7 and 8; Casellato and Erba, 2021). The reliability of records relative to the calpionellid and magnetostratigraphic framework may be assessed using Figures 7 and 8.

PALAEOMAGNETISM

SAMPLING METHOD AND LABORATORY EQUIPMENT

The sampling method was to take drilled or hand samples (as described in Bakhmutov et al., 2018). Palaeomagnetic measurements were performed in the laboratory of the Institute of Geophysics of the National Academy of Sciences of Ukraine in Kyiv. Standard specimens in the form of cylinders (2.2 cm long and 2.5 cm in diameter) or cubes (2.0 cm) were cut: with 2–4 specimens taken from each sample. The vectors of characteristic remanent magnetization (ChRM) were isolated by both stepwise thermal (TD) and alternating field (AF) demagnetization, using the same procedures described in Bakhmutov et al. (2018). Natural remanent magnetization (NRM) measurements (spinner magnetometer JR-6) and demagnetization experiments were carried out in a magnetically shielded space (a low-field cage, MMLFC). Specimens were thermally demagnetized stepwise using an MMTD80 oven up to 600°C, with monitoring of magnetic susceptibility (MS) after each thermal demagnetization step in order to track mineralogical changes during thermal treatment. Duplicate specimens were subjected to AF demagnetization up to 100 mT using a *LDA-3A* demagnetizer. Demagnetization results were processed by multicomponent analysis of the demagnetization path (Kirschvink, 1980), using *Remasoft 3.0* software (Chadima and Hrouda, 2006). Magnetic susceptibility and anisotropy of magnetic susceptibility (AMS) were measured on all samples with a *MFK-1B* kappabridge.

RESULTS OF PALAEOMAGNETIC INVESTIGATION

As shown by the results of our earlier palaeomagnetic studies on the Dvuyakornaya Formation, the most informative results for identifying the NRM-components of magnetization were those obtained by thermal demagnetization of mudstone samples. The results for sections 2 and 4 (Fig. 9) were partially presented in Bakhmutov et al. (2018) (where they were numbered as section 1 and 2, respectively). Here we present new results for sections 1 and 3, and additional results for reinterpretation of section 4.

In sections 2, 3 and 4 we demagnetized mostly mudstone samples and a limited number of other samples taken from coarse limestones, grainstones, rudstones, breccia etc. In section 1 the samples were taken only from grainstones and rudstones.

The average values obtained from mudstones are 2÷7 mA/m for NRM and (200÷300) x 10^{-6} SI for MS, which is similar to values from overlying mudstones in the Dvuyakornaya Formation. The NRM and MS values of grainstones/rudstones in section 1 are characterized by a wide range, ~1÷30 mA/m for NRM and (140÷1000) x 10^{-6} SI for MS, and on average higher than in the overlying sections – 2, 3 and 4 (Fig. 9). The data coincides well with the peaks in MS and NRM obtained from the same outcrop shown by Guzhikov et al. (2012: fig. 8).

Multicomponent analysis of demagnetization paths reveals that the NRM of the samples display two or three components (Fig. 10). The LTC (low stability) component is isolated in the 120–240°C temperature range (Fig. 10A) or AF field in the interval 10–20 mT (Fig. 10B). The intermediate stability component (ITC) was erased in the temperature range of 240–400°(460°)C in some samples and is not pronounced in the AF demagnetization path. The most stable high-temperature components (HTC) in the temperature range from 400°(500°)–580°(600°)C are for most of the specimens towards to the end point on the orthogonal projections (Fig. 10A, C, D), and this is accepted as a characteristic component (ChRM). The high coercivity components (HCC) are not fully demagnetized, even when there are high values of AF (Fig. 10B).

Experiments of magnetic mineralogy have been carried out on a number of samples from the same sections, and these define the magnetite as the main NRM carrier in the studied rocks (Guzhikov et al., 2012). The magnetite grains were partially oxidized to maghemite, and some results demonstrate the presence of a hard coercivity mineral (probably hematite). Our demagnetization results confirm the presence of magnetite as the main carrier of magnetization, coincident with results obtained from the uppermost part of Dvuyakornaya Formation sections and evidence in favour of the primary magnetization of the ChRM-component (Bakhmutov et al., 2018). Thus we can explain that the variation in the unblocking temperature, mostly from 400 to 580°C, is due to presents of magnetite, and the high coercivity component is due to an authigenic secondary mineral (hematite) formed during subsequent diagenesis.

The LTC component (Fig. 11A) is exclusively of normal polarity and constitutes a significant portion of the NRM intensity, frequently reaching 50% and more of the initial NRM. The mean direction (Table 1) calculated for all samples (D = 347°, I = 59°) is not so far from the present-day geocentric axial dipole field (I = 63°) at the sampling locality, and it has been introduced by recent growth of viscous remanence. The ITC component also shows only normal polarity (Fig. 11B),

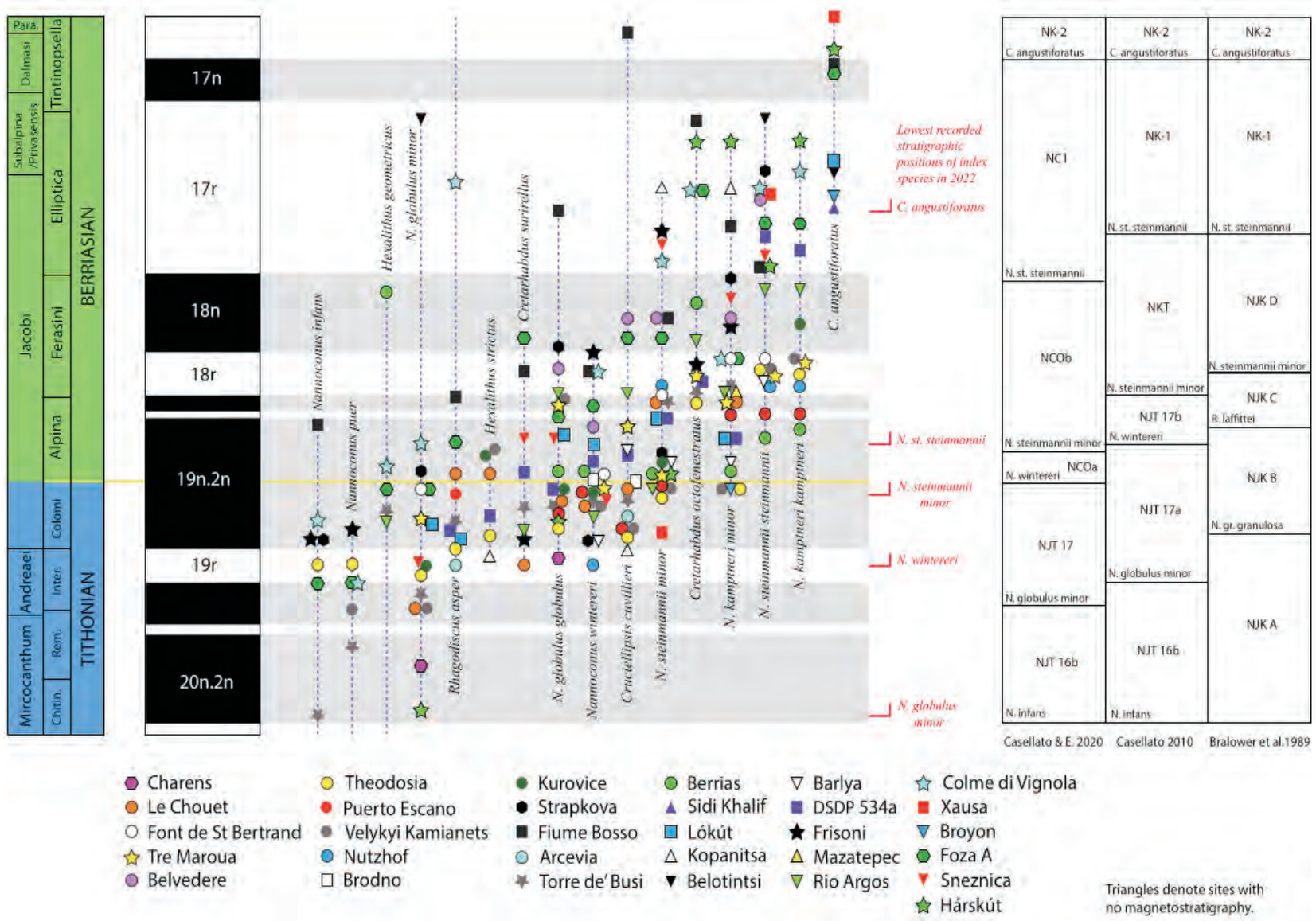

Fig. 7. Selected J/K sections showing calcareous nannofossil first occurrences

Sources for nannofossil data: Tre Maroua – Wimbledon et al. (2020d); Le Chouet – Wimbledon et al. (2013); Ravin de Font de St Bertrand – Wimbledon et al. (2020c); Charens – Wimbledon et al. (2020c); Puerto Escaño – Svobodova and Kostak (2016); Kurovice – Svobodova et al. (2019b); Strapkova – Michalik et al. (2016); Lók'ut and Hárskút – Lodowski et al. (2022); Berrias – Svobodova (unpubl.); Theodosia – Bakhmutov et al. (2018); Svobodova et al. (2019a); DSDP 534a – left Casellato and Erba (2021), right Bergen et al. (2013); Nutzhof – Lukeneder et al. (2010); Velykyi Kamianets – Grabowski et al. (2019); Kopanitsa – Stoykova et al. (2018); Xausa – Channell and Grandesso (1987); Frisoni – Channell et al. (2010); Fiume Bosso – Bralower et al. (1989); Rio Argos – Hoedemaeker et al. (2016); Torre de' Busi – Casellato and Erba (2020); Colme di Vignola – Channell et al. (2010); Foza – ditto; Brodno – Houša et al. (1996); Michalik et al. (2009). The ranges of calcareous nannofossils at Fiume Bosso are currently under revision, and in the meanwhile we only quote published records. In this figure, we record both *Hexalithus strictus* Bergen and *Hexalithus geometricus* Casellato: though we recognise that the two were synonymised by Howe (2017), and the latter taxon was seen as a junior synonym of *Nannoconus infans* by Varol and Bowman (2019)

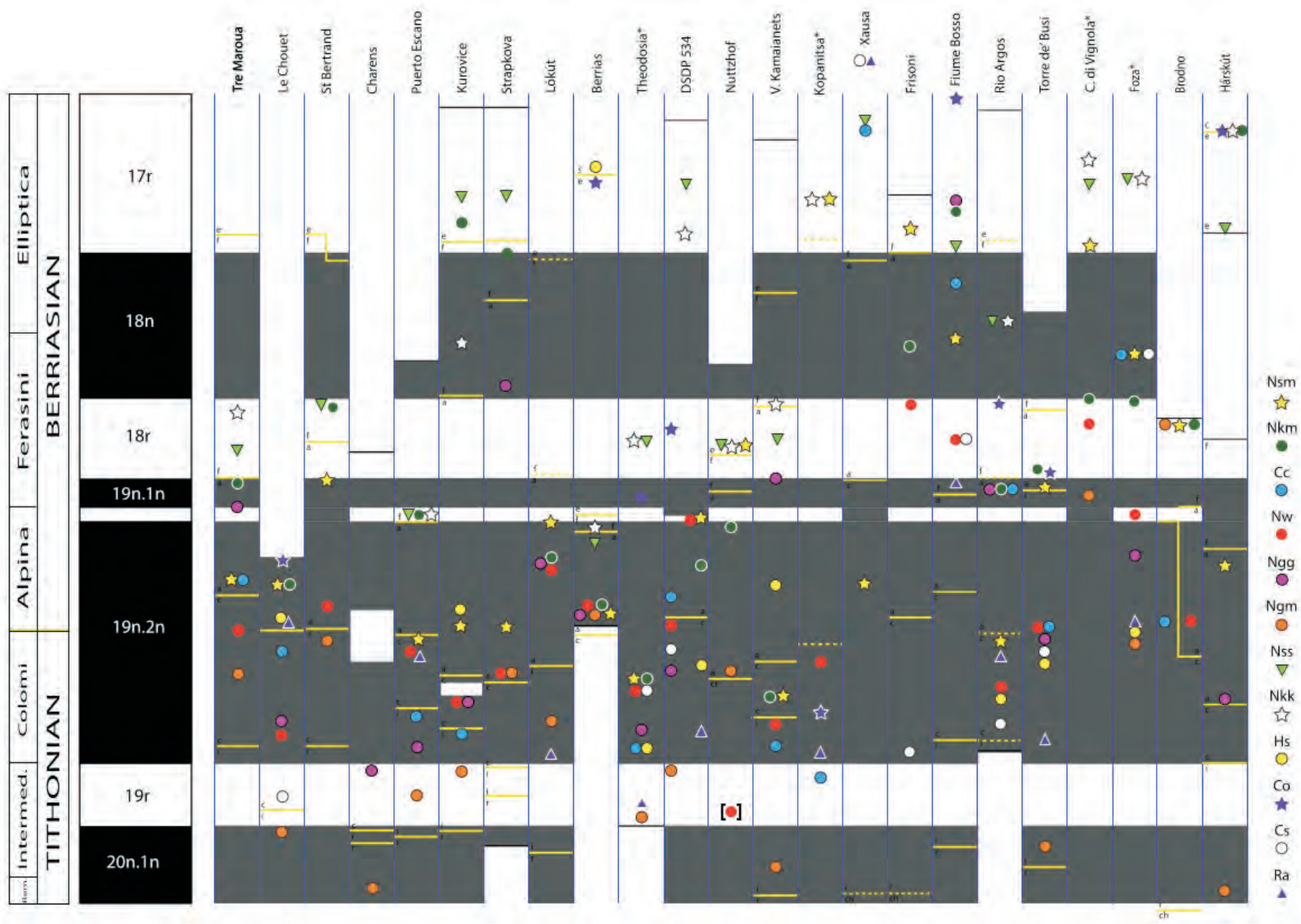

Fig. 8. First occurrences of selected calcareous nannofossil species in selected localities

Sites as listed in Figure 7, plus the following: Belvedere – Wimbledon et al. (2020c); Arcevia – Speranza et al. (2005); Sidi Khalif – Gardin, Wimbledon (unpubl.); Belotintsi – Lakova et al. (1999); Barlya – Grabowski et al. (2019); Mazatapec – Lopez-Martinez et al. (2013); Broyon – Bergen (1994); Sneznica – Michalik et al. (2019). Species abbreviations are as follows: Nsm – *Nannoconus steinmannii minor*, Nkm – *Nannoconus kamptneri minor*, Cc – *Cruciellipsis cuvillieri*, Nw – *Nannoconus wintereri*, Ngg – *Nannoconus globulus globulus*, Ngm – *Nannoconus globulus minor*, Nss – *Nannoconus steinmannii steinmannii*, Nkk – *Nannoconus kamptneri kamptneri*, Hs – *Hexalithus strictus*, Co – *Cretarhabdus octofenetratus*, Cs – *Cretarhabdus surirellus*, Ra – *Rhagodiscus asper*

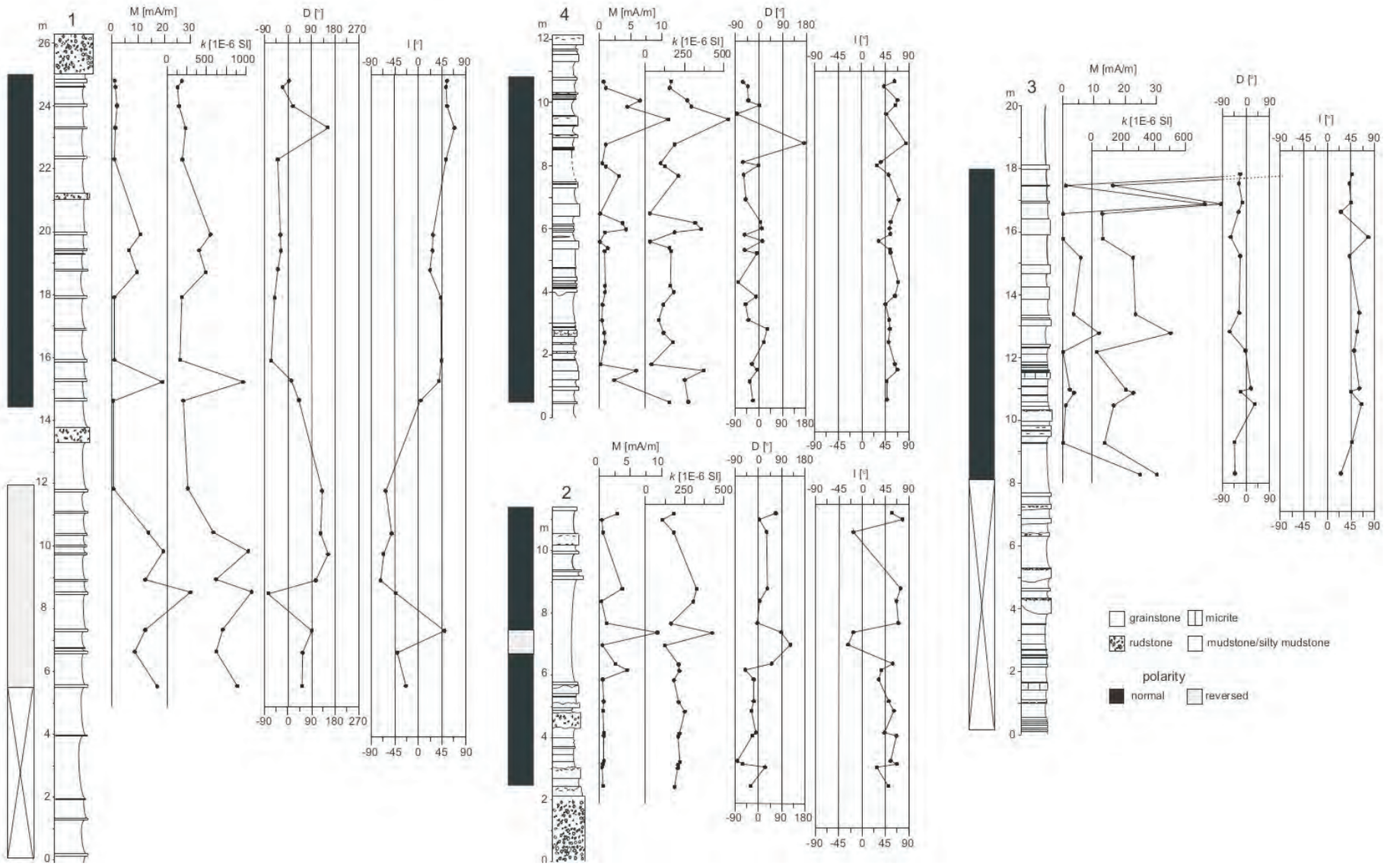

Fig. 9. Palaeomagnetic directions plotted through the sections

The direction of the ChRM-components (determined by the line fitting of the demagnetization path after temperature demagnetization and expressed by declination D° and inclination I°) plotted against the sample level

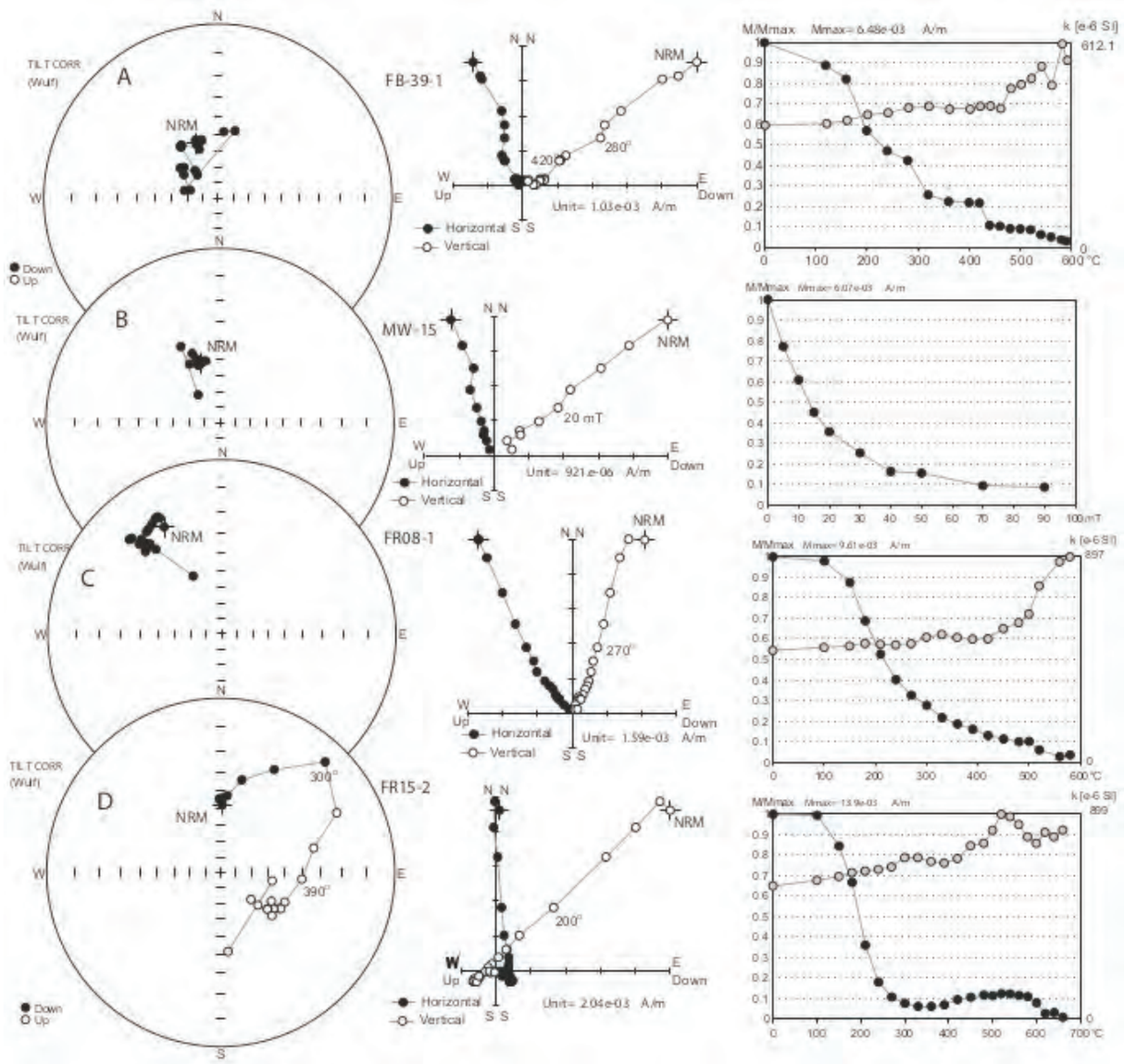

Fig. 10. Plots of the progressive thermal (A, C, D) and alternating field (B) demagnetization of mudstones (A, B) and grainstones (C, D) specimens

Left of diagram: stereographic projection of the directions (full and open circles represent projections in the lower and upper hemispheres, respectively); centre of diagram: orthogonal projections of demagnetization paths (Zijderveld diagrams) on horizontal and vertical planes (full and open circles respectively); right of diagram: NRM intensity (M/Mmax) and magnetic susceptibility (k) (black and grey circles respectively) decay during demagnetization; stereographic and orthogonal projections are given after tilt correction

with the average direction not far from the LTC component, and probably acquired in the Cenozoic (viscous origin). The HTC (ChRM) component has normal polarity in sections 4, 3, in most of section 2 and in the upper part of section 1 (Fig. 11C). In the lower part of section 1 this component has a reversed polarity direction (Fig. 11D and Table 1), except for one sample at the 7 metre level. We have to note that the sampling in section 1 was only from hard limestone layers, which have characteristically poorer palaeomagnetic qualities as compared to clays (Guzhikov et al., 2012; Bakhmutov et al., 2018). Taking into account the coincidence of MS and NRM data and the evidence of the consistency of our palaeomagnetic results from section 1 with those obtained by Guzhikov et al. (2012), we can precisely correlate the sampling levels in this outcrop.

MAGNETOSTRATIGRAPHY

The directions of HTC components of specimens (declinations and inclinations) and polarity are shown in Figure 9. The presence of normal and reversed HTC-component (which coincide in lithologically different sediments) and identification of magnetite (partially oxidized to maghemite) as the main carrier of remanent magnetization are the arguments in favour of the primary magnetization of the ChRM component, which could have formed during sedimentation or in an early stage of diagenesis.

Thus, sections 2, 3 and 4 have continuously normal polarity interval except two specimens on the middle part of section 2 with reverse polarity (Fig. 9). The upper part of section 1 also has normal polarity, but the lower part has reversed polarity.

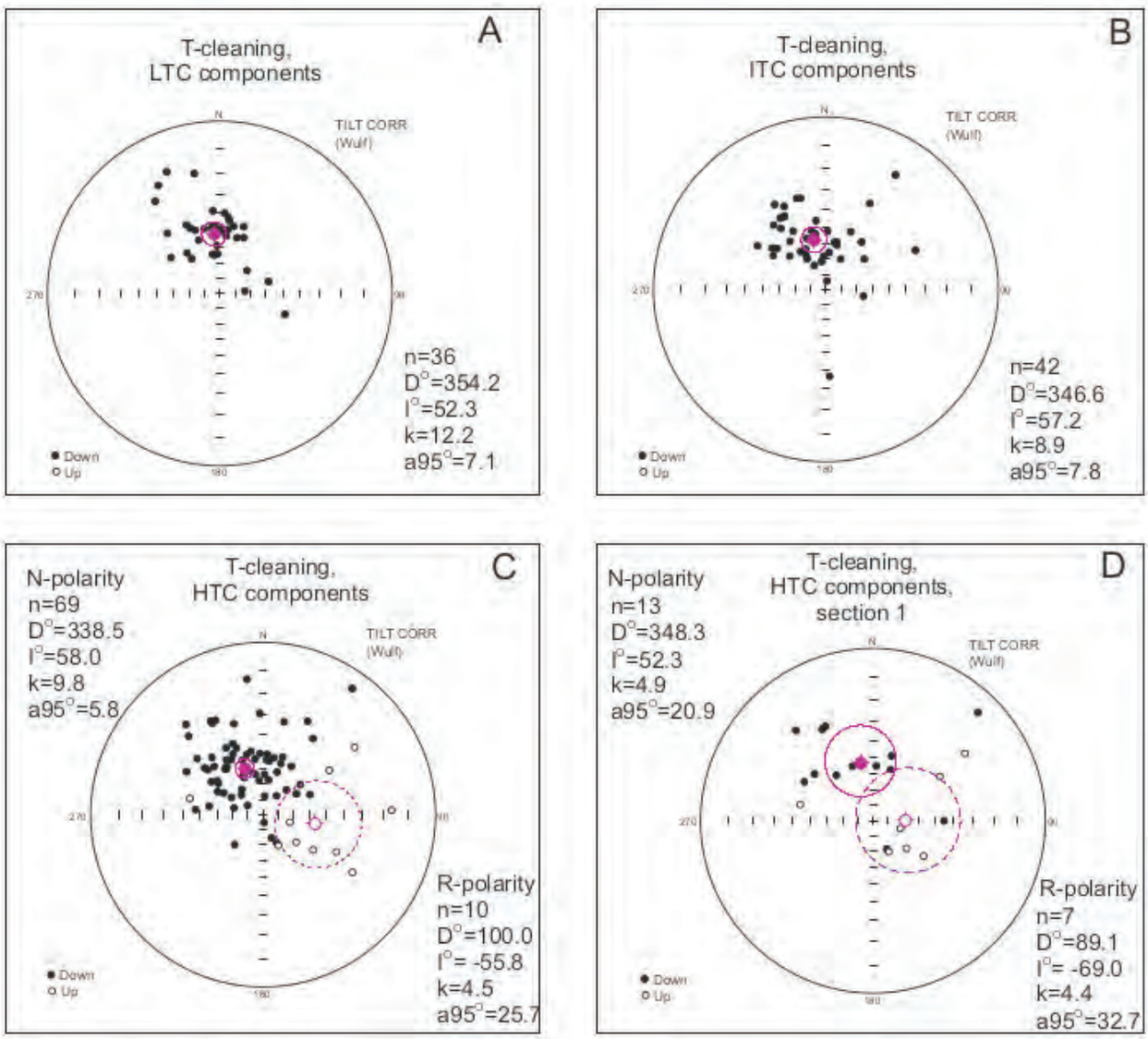

Fig. 11. Stereographic projections of corrected bedding dip directions of the LTC (A), ITC (B), HTC-components of all samples from sections 1, 2, 3, 4 and mudstone (a, b, c) and HTC-components from section1 (D) (Table 1)

Open symbols denote upward- and solid denote downward-pointing inclinations; the mean direction with radius of the 95% confidence cone and statistic parameters (n – number of specimens which yielded the components, D – mean declination, I – mean inclination, k – estimate of Fisher's precision parameter, $_{95}$ – half-angle of cone of 95% confidence, in degrees) are given for normal and reversed polarities

Our data from section 1 (Svobodova et al., 2019a and herein) agree well with results of normal and reversed polarities from the same outcrop presented by Guzhikov et al. (2012: fig. 4 members 7 and 8) but not with the numbering of magnetozones devised by Arkadiev et al. (2019), assigning middle Tithonian ammonites to a Berriasian "M19n.1r".

CONCLUSION

Despite concerns about identified inconsistencies with species first occurrences, the usefulness of nannofossils as stratigraphic indicators has been proved in more recent studies on profiles encompassing magnetozones M20-M17. In Crimea, our earlier work indicated the position of the J/K boundary in the Gulley section at Ili Burnu (Bakhmutov et al., 2018) – employing finds of nannofossil species used as proxies for the base of the *Calpionella alpina* Subzone. However, some uncertainty remained, as there existed unexposed ground between the Gully section (Fig. 1: column 4) and the Breccia section (Fig. 1: column 2), the lowest exposed part of the Ili Burnu sequence. In this account we remedy that situation, with the description of a stratigraphically intervening section (Fig. 1: column 3). The nannofossil occurrences, related to magnetozones, indicate that the earlier positioning of the base of the Berriasian (founded on the first occurrences of *N. steinmannii minor* and *N. kamptneri minor*, in particular) was correct. The new section yields *N. globulus globulus* and *Cruciellipsis cuvillieri* (the latter already identified in the underlying Breccia

Table 1

Directions of the particular NRM components of samples before and after tilt correction

Component of NRM	n	Directions expressed in geographic coordinates				Bedding-tilt corrected directions			
		D [°]	I [°]	k	α_{95} [°]	D [°]	I [°]	k	α_{95} [°]
LTC	36	347.2	58.6	14.7	6.5	354.2	52.3	12.2	7.1
ITC	42	336.8	60.1	8.9	7.9	346.6	57.2	8.9	7.8
HTC									
Normal	69	328.3	60.2	10.2	5.7	338.5	58.0	9.8	5.8
Reversed	10	79.4	–51.9	4.5	25.9	100.1	–55.8	4.4	25.7
HTC (section 1 – FR)									
Normal	13	336.7	65.8	6.1	18.3	348.3	52.3	4.9	20.9
Reversed	7	58.8	–60.6	4.4	32.6	89.1	–69.0	4.4	32.7

For explanations see Figure 11

section), and doubtfully identified *N. wintereri*, which, in the absence of *N. steinmannii minor* and *N. kamptneri minor*, indicate that the identified normal magnetic interval is indeed the lower half of M19n.2n. This is reinforced by the identification 3 km to the west (Fig. 1: section 1) of the presumed base of M19n.2n and the uppermost portion of M19r.

Acknowledgements. The authors would like to thank A. Guzhikov and two anonymous reviewers for their valuable comments and improvements of the manuscript. The nannofossil investigations were funded by the Czech Science Foundation (GAČR) project No 20-10035S and institutional support RVO 67985831.

REFERENCES

Arkadiev, V.V., Lescano, M., Concheyro, A., Guzhikov, A., Baraboshkin, E., 2019. The calcareous nannofossils and magnetostratigraphic results from the Upper Tithonian–Berriasian of Feodosiya region (Eastern Crimea). Geologica Carpathica, **70**: 355–369.

Bakhmutov, V.G., Casellato, C.E., Halásová, E., Ivanova, D.K., Reháková, D., Wimbledon, W.A.P., 2016. Bio- and magnetostratigraphy of the Upper Tithonian–Lower Berriasian in Southern Ukraine. In: Workshop of the ICS Berriasian Group and IGCP 632 (eds. J. Michalík and K. Fekete): 97–100. Field Trip Guide and Abstracts Book. Earth Science Institute, Slovak Academy of Sciences, Bratislava.

Bakhmutov, V.G., Halásová, E., Ivanova, D.K., Józsa, Š., Reháková, D., Wimbledon, W.A.P., 2018. Biostratigraphy and magnetostratigraphy of the uppermost Tithonian–Lower Berriasian in the Theodosia area of Crimea (southern Ukraine). Geological Quarterly, **62** (2): 197–236.

Bergen, J.A., 1994. Berriasian to early Aptian calcareous nannofossils from the Vocontian Trough (SE France) and Deep Sea Site 534: new nannofossil taxa and a summary of low-latitude biostratigraphic events. Journal of Nannoplankton Research, **16**: 59–69.

Bergen, J.A., Boesiger, T.M., Popischal, J.J., 2013. Low-latitude Oxfordian to Early Berriasian nannofossil stratigraphy and it application to the subsurface of eastern Texas and western Louisiana. AAPG Memoir, **105**: 69–102.

Bown, P.R., 1992. New calcareous nannofossil taxa from the Jurassic/Cretaceous boundary interval of sites 765 and 261, Argo Abyssal Plain. Initial Reports of the Ocean Drilling Program, Scientific Results, **123**: 369–379.

Bown, P.R., Cooper, M.K.E., 1998. Jurassic. In: Calcareous Nannofossil Biostratigraphy (ed. P.R. Bown): 34–85. British Micropalaeontological Society, London.

Bralower, T.J., Monechi, S., Thierstein, H.R., 1989. Calcareous nannofossil zonation of the Jurassic–Cretaceous boundary interval and correlation with the geomagnetic polarity timescale. Marine Micropaleontology, **14**: 153–235.

Casellato, C.E., 2010. Calcareous nannofossil biostratigraphy of Upper Callovian–Lower Berriasian successions from Southern Alps, North Italy. Rivista Italiana di Paleontologia e Stratigrafia, **116**: 357–404.

Casellato, C.E., Erba, E., 2021. Reliability of calcareous nannofossil events in the Tithonian-early Berriasian time interval: implications for a revised high resolution zonation. Cretaceous Research, **117**: 104611,

Chadima, M., Hrouda, F., 2006. Remasoft 3.0 – a user-friendly paleomagnetic data browser and analyzer. Travaux Géophysiques, 27: abstracts of the 10th “Castle Meeting”. New Trends in Geomagnetism. Castle of Valtice, September 3–8th, 2006: 20–21.

Channell, J.E.T., Grandesso, P., 1987. A revised correlation of Mesozoic polarity chrons and calpionellid zones. Earth and Planetary Science Letters, **85**: 222–240.

Channell, J.E.T., Casellato, C.E., Muttoni, G., Erba, E., 2010. Magnetostratigraphy, nannofossil stratigraphy and apparent polar wander for Adria-Africa in the Jurrasic-Cretaceous boundary interval. Palaeogeography, Palaeoclimatology, Palaeoecology, **293**: 51–75.

Frau, C., Bulot, B.G., Reháková, D., Wimbledon, W.A.P., 2016. Revision of the ammonite index species *Berriasella jacobi* Mazenot, 1939 and its consequences for the biostratigraphy of the Berriasian Stage. Cretaceous Research, **66**: 94–114.

Grabowski, J., Bakhmutov, V., Kdyr, S., Krobicki, M., Pruner, P., Schnabl, P., Stoykova, K., Wierzbowski, H., 2019. Integrated stratigraphy and palaeoenvironmental interpretation of the Upper Kimmeridgian to Lower Berriasian pelagic sequences of the Velykyi Kamianets section (Pieniny Klippen Belt, Ukraine). Palaeogeography, Palaeoclimatology, Palaeoecology, **532**: 109216.

Gradstein, F.M., Waskowska, A., Kopaevich, L., Watkins, D.K., Friis, H., Panera, J., 2019. Berriasian planktonic foraminifera and calcareous nannofossils from the Crimea Mountains, with reference to microfossil evolution. Swiss Journal of Palaeontology, **138**: 213–236.

Guzhikov, A.Y., Arkad'ev, V.V., Baraboshkin, E.Y., Bagaeva, M.I., Piskunov, V.K., Rud'ko, S.V., Perminov, V.A., Manikin, A.G., 2012. New sedimentological, bio-, and magnetostratigraphic data on the Jurassic–Cretaceous boundary interval of Eastern Crimea (Feodosiya). Stratigraphy and Geological Correlation, **20**: 261–294.

Houša, V., Krs, M., Krsová, M., Pruner, P., 1996. Magnetostratigraphic and micropalaeontological investigations along the Jurassic/Cretaceous boundary strata, Brodno near Žilina (Western Slovakia). Geologica Carpathica, **47**: 135–151.

Hoedemaeker, P.J., Jannsen, N.M.M., Casellato, C.E., Gardin, S., Reháková, D., Jamrichova, M., 2016. Jurassic-Cretaceous boundary in the Río Argos succession (Caravaca, SE Spain). Revue de Paleobiogie, **35**: 111–247.

Howe, R.W., 2017. *Acadialithus*, a new nannofossil genus from offshore Eastern Newfoundland, Canada. Journal of Nannoplankton Research, **37**: 61–66.

Ivanik, M.M., Zhabina, N.N., Anikeeva, E.V., 2013. Features of the Tithonian-Berriasian of south-eastern Crimea (area of Cape St Elijah) (in Ukrainian with English summary). Heolohichnyi Zhurnal, (4): 33–45.

Kirschvink, J.L., 1980. The least squares line and plane and the analysis of palaeomagnetic data. Geophysical Journal of the Royal Astronomical Society, **62**: 699–718.

Lakova, I., Stoykova, K., Ivanova, D., 1999. Calpionellid, nannofossil and calcareous dinocyst events and integrated biochronology of the Tithonian to Valanginian in the Western Balkanides, Bulgaria. Geologica Carpathica, **50**: 151–168.

Lodowski, D.G., Pszczó³kowski, A., Szives, O., Fõzy, I., Grabowski, J., 2022. Jurassic–Cretaceous transition in the Transdanubian Range (Hungary): integrated stratigraphy and palaeomagnetic study of the Hárskút and Lókút sections. Newsletters in Stratigraphy, **55**: 99–135.

López-Martínez, R., Barragán, R., Reháková, D., 2013. The Jurassic/Cretaceous boundary in the Apulco area by means of calpionellids and calcareous dinoflagellates: an alternative to the classical Mazatepec section in eastern Mexico. Journal of South American Earth Sciences, **47**: 142–151.

Lukeneder, A., Halasova, E., Kroh, A., Mayrhofer, S., Pruner, P., Reháková, D., Schnabl, P., Sprovieri, M., Wagreich, M., 2010. High resolution stratigraphy of the Jurassic-Cretaceous boundary interval in the Gresten Klippen Belt (Austria). Geologica Carpathica, **61**: 365–381.

Matveyev, A.V., 2009. Tithonian Calcareous Nannoplankton of the Eastern Crimea. In: Fossil Flora and Fauna of Ukraine: Palaeoecological and Stratigraphic Aspects (in Ukrainian). Proceedings of the Institute of Geological Sciences of the National Academy of Sciences of Ukraine, Kiev: 104–107.

Matlai, L.M., 2011. Stratigraphic subdivision of Jurassic and Cretaceous boundary sections of East Crimea by calcareous nannoplankton (in Ukrainian). Transactions National Academy Sciences of Ukraine, (1): 106–111.

Michalík, J., Reháková, D., Halásová, E., Lintnerová, O., 2009. The Brodno section – a potential regional stratotype of the Jurassic/Cretaceous boundary (Western Carpathians). Geologica Carpathica, **60**: 213–232.

Michalík, J., Reháková, D., Grabowski, J., Lintnerová, O., Svobodová, A., Schlögl, J., Sobieň, K., Schnabl, P., 2016. Stratigraphy, lithological and magnetic proxies of the Jurassic/Cretaceous boundary interval in the Pieniny Klippen Belt (Western Carpathians, Slovakia). Geologica Carpathica, **67**: 303–328.

Michalík, J., Reháková, D., Lintnerová, O., Gorièan, Š., Švábenická, L., Fekete, K., 2019. Snežnica section. In: 14th Jurassica Conference and Workshop of the ICS Berriasian Group – Field Trip Guide and Abstracts Book (eds. K. Fekete, J. Michalík and D. Reháková): 10–14. 14th Jurassica Conference and Workshop of the ICS Berriasian Group. Bratislava, Earth Science Institute, Slovak Academy of Sciences and Faculty of Natural Sciences, Comenius University.

Speranza, F., Satolli, S., Mattioli, E., Calamita, F., 2005. Magnetic stratigraphy of Kimmeridgian-Aptian sections from Umbria-Marche (Italy): new details on the M polarity sequence. Journal of Geophysical Research, **110**, B12109: 1–26.

Stoykova, K., Idakieva, V., Ivanov, M., Reháková, D., 2018. Calcareous nannofossil and ammonite integrated biostratigraphy across the Jurassic-Cretaceous boundary strata of the Kopanitsa composite section (West Srednogorie Unit, southwest Bulgaria). Geologica Carpathica, **69**: 199–217.

Švábenická, L., 2012. Nannofossil record across the Cenomanian–Coniacian interval in the Bohemian Cretaceous Basin and Tethyan foreland basins (Outer Western Carpathians), Czech Republic. Geologica Carpathica, **63**: 201–217.

Svobodová, A., Koš□ák, M., 2016. Calcareous nannofossils of the Jurassic-Cretaceous boundary strata in the Puerto EscaÔo section (southern Spain) – biostratigraphy and palaeoecology. Geologica Carpathica, **67**: 223–238.

Svobodová, A., Wimbledon, W.A.P., Bakhmutov, V.G., 2019a. New biostratigraphic and magnetostratigraphic data across the Jurassic–Cretaceous transition in the Theodosia area of Crimea (southern Ukraine). 14th Jurassica Conference and Workshop of the ICS Berriasian Group – Field Trip Guide and Abstracts Volume (eds. K. Fekete, J. Michalík and D. Reháková): 169. Earth Science Institute, Slovak Academy of Sciences, Bratislava.

Svobodová, A., Švábenická, L., Reháková, D., Svobodová, M., Skupien, P., Elbra, T., Schnabl, P., 2019b. The Jurassic/Cretaceous boundary and high resolution biostratigraphy of the pelagic sequences of the Kurovice section (Outer Western Carpathians, the northern Tethyan margin). Geologica Carpathica, **70**: 153–182.

Varol, O., Bowman, A.R., 2019. Taxonomic revision of selected Late Jurassic (Tithonian) calcareous nannofossils and the application of mobile mounting. Neues Jahrbuch für Geologie und Paläontologie Abhandlungen, **291**: 65–87.

Wimbledon, W.A.P., Reháková, D., Pszczó³kowski, A., Casellato, C.E., Halásová, E., Frau, C., Bulot, L.G., Grabowski, J., Sobieň, K., Pruner, P., Schnabl, P., Èížková, K., 2013. A preliminary account of the bio- and magnetostratigraphy of the upper Tithonian–lower Berriasian interval at Le Chouet, Drôme (SE France). Geologica Carpathica, **64**: 437–460.

Wimbledon, W.A.P., Reháková, D., Halásová, E., Lintnerová, O., Michalík, J., Pruner, P., Schnabl, P., Èízková, K., Koš□ák, M., Svobodová, A., Bulot, L.G., Frau, C., Bakhmutov, V., Grabowski, J., Wierzbowski, A., Pszczo³kowski, A., Leanza, H., Riccardi, A., Vennari, V., Aguirre-Uretta, B., Tchoumatchenko, P., Stoykova, K., Ivanova, D., Sha, J., Li, G., Meizhen, C., Jianguo, L., Xiaoqiao, W., Riding, J., Hunt, C., Rawson, P., Copestake, P., Arnaud-Vanneau, A.M., Mohialdeen, I.J., Andreini, G., Parisi, G., Speranza, F., Satolli, S., Martinez, R.L., Barragan, R., Benzaggagh, M., Verreussel, R., Munsterman, D., Hoedemaeker, P., Vajda, V., Erba, E., Casellato, C., Bown, P., Pandey, K., Fözy, I., Bardhan, S., Mojon, P.O., Sames, B., Lakova, I., Ivanov, M., Poulton, T.P., Galloway, J., Haggart, J.W., Davies, E.H., Alsen, P., Piacecki, S., Gardin, S., Galbrun, B., Ogg, J.G., Lucas-Clark, J., Pujana, I., Yondon, K., Olóriz, F., 2017a. The Tithonian/Berriasian stage boundary and the base of the Cretaceous System. In: 10th International Symposium on the Cretaceous. Vienna, August 21–26, 2017. Berichte der Geologischen Bundesanstalt, **120**: 290.

Wimbledon, W.A.P., Bakhmutov, V.G., Halásová, E., Reháková, D., Ivanova, D., 2017b. Magnetostratigraphy constrained by biostratigraphy: the lower Berriasian of the Theodosia coast of southern Ukraine. 10th International Symposium on the Cretaceous. Vienna, August 21–26, 2017. Berichte der Geologischen Bundesanstalt: **120**: 291.

Wimbledon, W.A.P., Bakhmutov, V.G., Halásová, E., Svobodová, A, Reháková, D., Frau, C., Bulot, L.G., 2020a. Comments on the geology of the Crimean Peninsula and a reply to a recent publication on the Theodosia area by Arkadiev et al. (2019): "The calcareous nannofossils and magnetostratigraphic results from the Upper Tithonian-Berriasian of Feodosiya region (Eastern Crimea)". Geologica Carpathica, **71**: 516–525.

Wimbledon, W.A.P., Reháková, D., Svobodová, A., Elbra, T., Schnabl, P., Pruner, P., Šifnerová, K., Kdýr, Š., Dzyuba, O., Schnyder, J., Galbrun, B., Košák, M., Vaòková, L., Copestake, P., Hunt, C.O., Riccardi, A., Poulton, T.P., Bulot, L.G., Frau, C., De Lena, L., 2020b. The proposal of a GSSP for the Berriasian Stage (Cretaceous System): part 1. Volumina Jurassica, **18**: 53–106.

Wimbledon, W.A.P., Reháková, D., Svobodová, A., Schnabl, P., Pruner, P., Elbra, T., Èížková, K., Kdýr, Š., Frau, C., Schnyder, J., Galbrun, B., 2020c. Fixing a J/K boundary: a comparative account of key Tithonian-Berriasian profiles in the departments of Drôme and Hautes-Alpes, France. Geologica Carpathica, **71**: 24–46.

Wimbledon, W.A.P., Reháková, D., Svobodová, A., Elbra, T., Schnabl, P., Pruner, P., Šifnerová, K., Kdýr, Š., Schnyder, J., Galbrun, B., Vaòková, L., Copestake, P., Hunt, C.O., Riccardi, A., Poulton, T.P., Bulot, L.G., Frau, C., De Lena, L., 2020d. The proposal of a GSSP for the Berriasian Stage (Cretaceous System): part 2. Volumina Jurassica, **18**: 121–160.

Young, J.R., Bown, P.R., Lees, J.A. eds., 2017. Nannotax3 website. International Nannoplankton Association. Accessed 21 Apr. 2017. URL: https://www.mikrotax.org/Nannotax3

APPENDIX 1
LIST OF CALCAREOUS NANNOFOSSILS TAXA

Acadialithus dennei Howe, 2017
Assipetra infracretaceae (Thierstein, 1973) Roth, 1973
Biscutum constans (Górka, 1957) Black in Black and Barnes, 1959
Biscutum melaniae (Górka, 1957) Reinhardt, 1969
Conusphaera mexicana subsp. *mexicana* Trejo, 1969
Conusphaera mexicana subsp. *minor* Bown and Cooper, 1989
Cretarhabdus conicus Bramlette and Martini, 1964
Cruciellipsis cuvillieri (Manivit, 1966) Thierstein, 1971
Cyclagelosphaera argoensis Bown, 1992
Cyclagelosphaera deflandrei (Manivit, 1966) Roth, 1973
Cyclagelosphaera margerelii Noël, 1965
Diazomatolithus galicianus de Kaenel and Bergen, 1996
Diazomatolithus lehmanii Noël, 1965
Discorhabdus ignotus (Górka, 1957) Perch-Nielsen, 1968
Faviconus multicolumnatus Bralower in Bralower et al., 1989
Ethmorhabdus gallicus Noël, 1965
Hexapodorhabdus cuvillieri Noël, 1965
Helenea chiastia Worsley, 1971
Helenea staurolithina Worsley, 1971
Hexalithus geometricus Casellato, 2010
Hexalithus noeliae Loeblich and Tappan, 1966
Lotharingius hauffii Grün and Zweili in Grün et al., 1974
Manivitella pemmatoidea (Deflandre in Manivit, 1965) Thierstein, 1971
Micrantholithus parvistellatus Varol, 1991
Miravetesina favula Grün in Grün and Alleman, 1975
Nannoconus sp. Kamptner, 1931
Nannoconus bronnimannii Trejo, 1959
Nannoconus compressus Bralower and Thierstein in Bralower et al., 1989
Nannoconus dolomiticus Cita and Pasquare, 1959
Nannoconus globulus subsp. *globulus* Brönnimann, 1955
Nannoconus globulus subsp. *minor* Bralower in Bralower et al., 1989
Nannoconus infans Bralower in Bralower et al., 1989
Nannoconus puer Casellato, 2010
? Nannoconus steinmannii subsp. *minor* Deres and Achéritéguy, 1980
? Nannoconus wintereri Bralower and Thierstein, in Bralower et al., 1989
Parhabdolithus marthae Deflandre in Deflandre and Fert, 1954
Parhabdolithus robustus Noël, 1965
Polycostella beckmannii Thierstein, 1971
Polycostella senaria (Thierstein, 1971) Varol and Bowman, 2019
Polycostella senaria SV (= *Nannoconus erbae* Casellato, 2010) Varol and Bowman, 2019
Retecapsa sp. Black, 1971
Rhagodiscus asper (Stradner, 1963) Reinhardt, 1967
Staurolithites sp. Caratini, 1963
Thoracosphaera *operculata* Bramlette and Martini, 1964
Umbria granulosa subsp. *granulosa* Bralower and Thierstein in Bralower et al., 1989
Umbria granulosa subsp. *minor* Bralower and Thierstein in Bralower et al., 1989
Watznaueria barnesiae (Black in Black and Barnes, 1959) Perch-Nielsen, 1968
Watznaueria biporta Bukry, 1969
Watznaueria britannica (Stradner, 1963) Reinhardt, 1964
Watznaueria cynthae Worsley, 1971
Watznaueria fossacincta (Black, 1971) Bown in Bown and Cooper, 1989
Watznaueria moshkovitzii Varol and Bowman (2019)
Watznaueria ovata Bukry, 1969
Zeugrhabdotus sp. Reinhardt, 1965
Zeugrhabdotus cooperi Bown, 1992
Zeugrhabdotus embergeri (Noël, 1965) Perch-Nielsen, 1984
Zeugrhabdotus erectus (Deflandre in Deflandre and Fert, 1954) Reinhardt, 1965
Zeugrhabdotus fissus Grün and Zweili, 1980
Zeugrhabdotus fluxus Casellato, 2010
Zeugrhabdotus noeliae Rood et al., 1971